fishes

MDPI

Article

Probiotics Alleviate Nonylphenol-Induced Hepatotoxicity in *Silurus meridionalis* via Reprogramming Arachidonic Acid Metabolism and Suppressing Ferroptosis: A Preliminary Study

Deqin Luo [1], Fanglian Lu [1], Lian Yang [1], Zhenbo Gan [1], Xianbo Zhang [2] and Ranran Dong [1,*]

[1] College of Animal Science, Guizhou University, Guiyang 550025, China
[2] Guizhou Academy of Agricultural Sciences, Guiyang 550025, China
* Correspondence: rrdong@gzu.edu.cn; Tel.: +86-182-8607-9830

Abstract

Nonylphenol (NP), a typical emerging pollutant, is widely detected in water bodies, yet its hepatotoxic mechanisms and mitigation strategies remain underexplored. This study evaluated the protective effects of a mixed probiotic (*Lactobacillus acidophilus* and *Bacillus subtilis*) against NP-induced hepatotoxicity in *Silurus meridionalis* by integrating transcriptomic and metabolomic analyses, with validation by RT-qPCR and ELISA. The results showed that NP exposure disrupted the arachidonic acid (AA) pathway (activating pro-inflammatory COX and LOX pathways while the suppressing anti-inflammatory CYP450 branch), promoted ferroptosis via iron dyshomeostasis and oxidative damage, and impaired triglyceride (TG) synthesis. Probiotic pretreatment reversed these toxic effects by modulating AA metabolism, suppressing COX (*ptgs2a*↓ → PGE_2↓) and LOX (*alox12*↓ → MDA↓) pathways, while upregulating the CYP450 pathway (*cyp2j*↑ → 11,12-EET↑). Probiotics also enhanced Fe^{3+} sequestration (*steap4*↑) and antioxidant defense (CAT↑, *gpx4a*↑), limiting Fenton reaction-mediated oxidative injury, and restored hepatic TG synthesis through upregulation of the DHAP-to-TG cascade (DHAP—(*gpd1b*↑) → G3P↑—(*gpat3*↑) → LPA—(*agpat6*↑) → PA—(*plpp7*↑) → DAG↑—(*dgat2*↑) → TG↑). These findings suggest that NP induces hepatotoxicity in *S. meridionalis*, involving ferroptosis, AA metabolism disruption and impaired TG synthesis as interconnected pathological events. Probiotics likely counteract this toxicity through systemic metabolic reprogramming. Collectively, these findings elucidate the hepatotoxic mechanisms of NP in *S. meridionalis* and offer toxicological data for its risk assessment, supporting the potential of probiotic-based strategies to mitigate emerging pollutant impacts in aquatic organisms.

Keywords: nonylphenol; *Silurus meridionalis*; probiotics; arachidonic acid metabolism; triglyceride; ferroptosis

Key Contribution: This study demonstrates that nonylphenol hepatotoxicity in *Silurus meridionalis* involves arachidonic acid disruption, ferroptosis, and impaired triglyceride synthesis, while mixed probiotics (*L. acidophilus* and *B. subtilis*) reverse these effects via systemic metabolic reprogramming, providing a theoretical basis and practical reference for mitigating emerging pollutant impacts in aquaculture.

Check for updates

Academic Editor: Tin Klanjšček

Received: 13 July 2026
Revised: 10 August 2026
Accepted: 11 August 2026
Published: 13 August 2026

Copyright: © 2026 by the authors. Licensee MDPI, Basel, Switzerland. This article is an open access article distributed under the terms and conditions of the Creative Commons Attribution (CC BY) license.

1. Introduction

Nonylphenol (NP), a typical emerging pollutant, is ubiquitous in aquatic environments due to its persistence and widespread use as a degradation product of nonylphenol ethoxylates [1,2]. Once released, NP can destabilize aquatic ecosystems and impair fish health [3,4]. The liver, as the primary organ responsible for xenobiotic biotransformation, is particularly vulnerable to NP accumulation, which induces oxidative stress, inflammation, and apoptosis in fish [5]. However, the molecular mechanisms underlying NP hepatotoxicity in fish, particularly in benthic carnivorous species, remain insufficiently characterized.

In parallel, there is increasing interest in developing effective mitigation strategies against emerging pollutant toxicity. Probiotics, as green and safe micro-ecological regulators, have shown promise in alleviating environmental stress and pollutant-induced damage in aquatic organisms [6]. Among them, *Lactobacillus* and *Bacillus* species are widely used for their ability to modulate gut microbiota, enhance host defense, and regulate hepatic lipid metabolism [7,8]. Notably, the combination of *L. acidophilus* and *B. subtilis* has been reported to suppress inflammation in shrimp [9]. Additionally, a mixture of probiotics containing *L. acidophilus* and *B. subtilis* has been shown to enhance immunity and disease resistance in Nile tilapia (*Oreochromis niloticus*) [10]. However, whether the combination of *L. acidophilus* and *B. subtilis* can protect against NP-induced hepatotoxicity in fish remains unknown.

Silurus meridionalis is a benthic carnivorous species of high commercial value in China [11], and its bottom-dwelling habit makes it particularly susceptible to sediment-associated pollutants such as NP [12]. With the rapid expansion of intensive aquaculture, contaminants like NP have posed a significant threat to fish health [13]. Considering that the liver is critical for growth performance and survival of farmed fish [14], NP-induced hepatotoxicity in *S. meridionalis* and probiotic protection remain unexplored. Therefore, this study aimed to evaluate the protective effects and mechanisms of a mixed probiotic (*L. acidophilus* and *B. subtilis*) against NP-induced hepatotoxicity in *S. meridionalis* by integrating hepatic transcriptomic and metabolomic analyses with reverse transcription quantitative real-time PCR (RT–qPCR) and enzyme-linked immunosorbent assay (ELISA) validation. Our findings may provide mechanistic insights into NP hepatotoxicity in fish and offer a basis for considering probiotic-based strategies to mitigate the health impacts of emerging pollutants in aquatic organisms.

2. Materials and Methods

2.1. Chemicals, Probiotics, and Diet Preparation

Analytical-grade nonylphenol (NP; $C_{15}H_{24}O$; purity $\geq$ 99%; MW 220.35 g/mol; CAS No. 84852-15-3) from Macklin Biochemical Co., Ltd. (Shanghai, China), was dissolved in ethanol to create a 1 mg/mL stock solution, then diluted for exposure.

B. subtilis CGMCC No. 22175 (deposited by Jiangsu University) and *L. acidophilus* ATCC 4356 (originally isolated from human infant feces) powders, with viable cell counts of 1.0×10^{11} CFU/g and 1.0×10^{10} CFU/g, respectively, were purchased from Linyi Yiwu Anti-Biotechnology Co., Ltd. (Linyi, China). These probiotics were mixed in sterile water at a 1:1 (*w*/*w*) ratio and sprayed onto feed at a 1:100 probiotic-to-feed ratio. The feed was air-dried at room temperature and then stored at −20 °C in a sterile anaerobic environment [15,16].

2.2. Experimental Animals and Design

S. meridionalis (~20 cm) was obtained from an aquaculture farm in Huishui County, Guizhou Province, China. The total experimental period was 78 days (Supplementary Figure S1), consisting of 14 days of acclimation, 49 days of pre-exposure feeding (with or

without probiotic supplementation), and 15 days of NP exposure (0.1 mg/L) for designated groups [17,18]. The 49-day pre-feeding period was designed to ensure adequate probiotic colonization and host adaptation [19]. For acclimation, fish were kept in a freshwater recirculating system at 25–27 °C, and fed a commercial diet at 5% of their body weight twice daily. Water quality was maintained within pH 7.0 ± 0.5, dissolved oxygen ≥ 7.0 mg·L^{-1}, and water temperature 25.0 ± 2.0 °C, with 50% water renewal daily. After acclimation, fish were divided into four groups (20 fish each; abbreviated as Control, Probiotics, NP, and NP-Pro, respectively): (1) Control group: fed a basal diet without probiotics or NP exposure; (2) Probiotics group: fed a diet with 1% probiotics, no NP exposure; (3) NP group: fed a basal diet for 49 days, then 0.1 mg/L of NP for 15 days; (4) NP-Pro group: fed a diet with 1% probiotic-supplemented diet for 49 days, continued during 15-day NP exposure. All fish used in this study were handled in accordance with the institutional guidelines, following a protocol (code: EAE-GZU-2024-T103) approved by the Guizhou University Subcommittee of Experimental Animal Ethics. Fish were monitored twice daily (8:00 and 18:00) throughout the 78-day study . Humane endpoints (loss of balance, immobility, unresponsiveness, or abnormal ventilation) were predefined, but no fish met these criteria during the experiment. Four fish died during the 14-day acclimation period and were excluded from all analyses. At sampling, fish were euthanized by overdose of MS-222 (tricaine methanesulfonate) anesthesia. All efforts were made to minimize animal suffering and to reduce the number of animals used, and animal welfare was optimized throughout the experiment by improving housing and handling practices.

2.3. Sample Collection

After the feeding trial, all fish were fasted for 24 h prior to sampling. Each group consisted of three replicate tanks, with the tank as the experimental unit. At sampling, fish were anesthetized with MS-222 (200 ± 10 mg·L^{-1}) prior to tissue collection. Three fish were collected from each tank, yielding nine fish per group, and their livers were excised. Within each tank, one liver was divided into two equal portions for transcriptomics (n = 3) and RT-qPCR (n = 3), respectively; a second liver was used for untargeted metabolomics (n = 3); and the remaining liver was used for antioxidant indicator assays (n = 3). Each assay's three samples originated from three independent tank replicates [20,21]. All liver samples were immediately frozen in liquid nitrogen and stored at −80 °C.

2.4. Determination of Hepatic Oxidative Stress Parameters

Hepatic oxidative stress and antioxidant-related parameters were determined using commercial assay kits purchased from Saiyan Biotechnology Technology Co., Ltd. (Nanjing, China). The measured indices included superoxide dismutase (SOD), hydrogen peroxide (H_2O_2), malondialdehyde (MDA), and catalase (CAT), following the manufacturers' guidelines.

2.5. Hepatic Transcriptomic Analysis

RNA was extracted from liver tissues using the MJZol Total RNA Extraction Kit (Meiji Bio-Pharmaceutical Technology Co., Ltd., Shanghai, China). For transcriptomic analysis, three liver samples per group were randomly selected, and RNA quality was assessed with a 5300 Bioanalyzer and NanoDrop. Only samples meeting specific criteria ($OD_{260/280}$ = 1.8–2.2, $OD_{260/230}$ ≥ 2.0, RNA quality number ≥ 6.5, 28S/18S ratio ≥ 1.0, and >1 μg total RNA) were used for library construction, and selected samples met these criteria. mRNA libraries were created using the Illumina® Stranded mRNA Prep protocol. Briefly, poly(A)$^+$ mRNA was enriched with oligo(dT) magnetic beads, fragmented, and converted into cDNA. Libraries were PCR-amplified after end repair and adapter ligation. Library concentration determination was performed using a Qubit 4.0 (Thermo Fisher

Scientific, Waltham, MA, USA), and paired-end sequencing (PE150) was performed on the NovaSeq X Plus (Illumina, Inc., San Diego, CA, USA). Raw sequencing reads underwent quality control with fastp, were aligned to the reference genome using HISAT2, and were assembled with StringTie. Gene expression levels were quantified in TPM using RSEM, and differentially expressed genes (DEGs) were identified using DESeq2 and DEGseq ($|\log_2 FC| \geq 1$, FDR < 0.05). Only overlapping DEGs from both methods were retained for downstream analyses to reduce false positives [22]. Functional annotation and enrichment analyses of DEGs were performed using Gene Ontology (GO; Goatools) and Kyoto Encyclopedia of Genes and Genomes (KEGG; Python SciPy (v1.16.3)), with Bonferroni-corrected p-values < 0.05 deemed significant.

2.6. Metabolomic Analysis

Metabolomic analysis was performed on liver samples (50 mg) extracted with methanol–water (4:1, v/v). Pooled quality control (QC) samples were injected every 10 runs to monitor system stability and reproducibility; features with RSD > 30% were excluded. PCA of QC samples confirmed negligible instrumental drift. LC–MS/MS analysis was conducted using a UHPLC-Q Exactive HFX system with an HSS T3 column (100 × 2.1 mm, 1.8 μm). Mobile phases were water/acetonitrile (95:5) and acetonitrile/isopropanol/water (47.5:47.5:5), both with 0.1% formic acid. Data were acquired in positive and negative ESI modes over m/z 70–1050, and raw data were processed with Progenesis QI (v3.0). Metabolites were identified using accurate mass (<10 ppm) and MS/MS fragmentation against HMDB, METLIN, and an inhouse database. Features with >80% missing values were removed, with the remaining missing values being imputed with the minimum. Data were normalized to total ion intensity, and features with RSD >30% in QCs were excluded, and Log_{10} transformation was applied. Multivariate analyses (PCA, OPLSDA) were performed using the ropls package in R. The permutation test results (200 permutations) showed Q^2 values of 0.72 (positive) and 0.79 (negative), and R^2Y intercepts below 0.3, confirming that the OPLS-DA models have good predictive performance without overfitting. Differential metabolites required VIP > 1.0 and $|\text{Log}_2 FC| \geq 1$ [23]. Pathway enrichment was conducted with KEGG and Fisher's exact test.

2.7. Validation of DEGs Using Reverse Transcription Quantitative Real-Time PCR (RT-qPCR) Validation of DEGs

To validate the transcriptomic data, five DEGs were analyzed using RT-qPCR. RNA was extracted from liver tissues using the TRIzol® Plus RNA Purification Kit (Thermo Fisher Scientific, Waltham, MA, USA) and treated with an RNase-Free DNase Set (Qiagen, Hilden, Germany) to eliminate genomic DNA. First-strand cDNA was synthesized using the SuperScript™ III First-Strand Synthesis SuperMix (Thermo Fisher Scientific, USA). Gene-specific primers were designed using Primer Premier 6.0, and *β-actin* was used as the internal reference gene (Table 1), and its expression stability was verified by consistent Ct value consistency across groups ($p > 0.05$ for all pairwise comparisons). Primers were synthesized by Sangon Biotech (Shanghai, China). RT-qPCR assays were performed using Power SYBR® Green PCR Master Mix (Applied Biosystems, Waltham, MA, USA) on a CFX384 real-time PCR detection system (Bio-Rad, Hercules, CA, USA). The amplification protocol consisted of an initial denaturation at 95 °C for 1 min, followed by 40 cycles of denaturation at 95 °C for 15 s and annealing/extension at 60 °C for 25 s. All reactions were conducted in triplicate. Relative gene expression levels were calculated using the $2^{-\Delta\Delta Ct}$ method.

Table 1. Reverse transcription quantitative real-time PCR (RT-qPCR) primers and conditions.

Gene	Gene ID	Primer Sequences (5′ to 3′)	Size (bp)	Annealing (°C)
β-actin	124385997	CCTGACGGACAGGTCATCA CGGATGTCGACATCACACTTCA	143	60
cat	124392486	CTCCATCCGTGACCTGTACAAC CGAATGGGTTCCATGGGTACTTCT	113	60
gpx4a	124390796	CCAGGAGCCTGGTACACAT GTTGACCCTGACCTTGCTGA	88	60
hpxa	124382666	CAGCCATGTGCACCTGGAT GCATCGATGTCATCATGAAGACCT	150	60
igfbp1b	124387463	GGCGAGAAGTTCACCACGTT GACGAGAGACGTCTCACACT	84	60
sod1	124393825	TGGGTCTGATGGAGTTGCTCA CCTCCTTCTCATGAATCACCATG	104	60

2.8. Statistical Analysis

Data are shown as mean ± standard deviation (SD). Statistical significance was assessed by one-way ANOVA and Tukey's test, with analyses conducted in GraphPad Prism software (version 9.5; GraphPad Software, San Diego, CA, USA). The difference was indicated by $p < 0.05$. Spearman's rank correlation analysis was performed on gene–metabolite pairs derived from DEGs and differential metabolites using Python (version 3.10.9). Significant correlations were defined as $|r| > 0.7$ with raw $p < 0.05$, followed by Benjamini–Hochberg false discovery rate (FDR) correction (FDR < 0.05). Only gene–metabolite pairs meeting these criteria were retained. KEGG pathway enrichment analysis was performed using the hypergeometric test (FDR < 0.05). Correlation heatmaps were generated using the Majorbio Cloud Platform (https://www.majorbio.com/tools) (accessed on 24 November 2025), and pathway figures were generated using Figdraw 2.0.

3. Results

3.1. Changes in Hepatic Oxidative Stress Parameters

NP exposure significantly altered hepatic oxidative stress in *S. meridionalis* (Table 2). Compared to the Control group, the NP group showed significantly decreased activities of SOD and CAT and increased MDA levels ($p < 0.05$). The NP-Pro group showed significantly higher SOD and CAT activities, as well as lower MDA and H_2O_2 levels, than the NP group ($p < 0.05$). In the Probiotics group, SOD activity was higher, while CAT activities and H_2O_2 and MDA levels were lower than those in the Control group ($p < 0.05$).

Table 2. Effects of NP and probiotics on hepatic indices of *S. meridionalis*. (mean ± SD, $n = 3$).

Parameters	Groups			
	Control	NP	NP-Pro	Probiotics
SOD (U/mL)	2.82 ± 0.15 ^{d}	2.24 ± 0.22 ^{c}	3.12 ± 0.13 ^{b}	3.42 ± 0.28 ^{a}
CAT (μmoL/min/mL)	101.27 ± 9.4 ^{a}	59.32 ± 10.8 ^{c}	79.81 ± 3.06 ^{b}	66.23 ± 3.50 ^{bc}
MDA (nmol/mL)	5.72 ± 0.03 ^{a}	6.87 ± 0.08 ^{c}	3.95 ± 0.03 ^{d}	5.15 ± 0.28 ^{b}
H_2O_2 (μmoL/mL)	0.15 ± 0.01 ^{a}	0.17 ± 0.02 ^{b}	0.07 ± 0.01 ^{c}	0.05 ± 0.01 ^{c}

Note: Different superscript letters within the same row indicate significant differences between groups ($p < 0.05$); identical letters indicate no significant difference ($p > 0.05$).

3.2. Transcriptional Restoration by Probiotics in NP-Exposed S. meridionalis

Probiotics intervention effectively alleviated NP-induced transcriptional dysregulation and maintained host gene expression homeostasis. Firstly, in the NP group, genes like *ptgs2a* (encoding COX-2), *alox12*, and *steap4* were significantly up-regulated ($p < 0.05$). Concurrently, lipid metabolism genes including *acsl4a*, *dgat1b*, *gpd1b*, *agpat6*, *gpat3*, *plpp7a* and *cyp2j* were significantly suppressed ($p < 0.05$) (Figure 1A). Secondly, probiotics intervention exhibited a significant antagonistic effect. Volcano plot analysis of the "NP-Pro vs. NP" groups ($|\mathrm{Log_2FC}| \geq 1$, adjusted $p < 0.05$) revealed that the expression of *ptgs2a*, *alox12*, and *steap4* was significantly downregulated ($p < 0.05$). Conversely, the expression levels of *acsl4a*, *dgat2*, *agpat6*, *gpat3*, *plpp7*, *cyp2j*, *sod1*, *cat*, *gpx4a*, and *hpxa* were significantly upregulated in the NP-Pro group ($p < 0.05$) (Figure 1B). Finally, Venn diagram analysis of the DEGs among the three groups identified 47 core DEGs (Figure 1C).

3.3. Probiotics Restore NP Altered Hepatic Metabolic Profiles

Metabolomic analysis further confirmed the protective effect of probiotics. PCA revealed that NP exposure altered the hepatic metabolic profile of *S. meridionalis*, whereas probiotics (NP-Pro group) effectively restored it to resemble the Control group (Figure 2A). Volcano plot analysis (NP-Pro vs. NP) showed significant downregulation of ProstaglandinE2 (PGE_2), acylcarnitine (Car (6:1)), loganate, and kynurenic acid, alongside upregulation of glycerol-3-phosphate, 11,12-epoxyeicosatrienoic acid (11,12-EET), and galactonic acid (Figure 2B). Clustering analysis further identified PGE_2, glycerol-3-phosphate, 11,12-epoxyeicosatrienoic acid, galactaric acid, and sphingosine 1-phosphate as the key metabolites (VIP > 1) distinguishing the NP and NP-Pro metabolic profiles (Figure 2C).

3.4. Integrated Analysis Confirms Probiotic Reversal of NP-Induced Effects

Integrated transcriptomic and metabolomic analyses confirmed that probiotics supplementation effectively reversed the adverse effects of NP on host gene expression and metabolite production. The correlation heatmap revealed significant positive correlations between the genes (*gpd1b*, *dgat2*, *acsl4a*, *agpat6*, *gpat3*, *hpxa*, *steap4*, *alox12*, *ptgs2a* and *cyp2j*) and lipid metabolites such as glycerol-3-phosphate, PGE_2, 11,12-EET, 3-phosphoglycerate, and 6-phosphogluconic acid, indicating a synergistic relationship (Figure 3A). The gene–metabolite association network revealed significant correlations between key transcripts and multiple metabolites, involving both positive and negative interactions. *cyp2j*, *gpd1b*, *dgat2*, *ptgs2a*, and *alox12* emerged as central nodes, connecting to hub metabolites including glycerol3phosphate, PGE_2, 11,12EET, and 3-phosphoglycerate (Figure 3B). KEGG pathway enrichment analysis of the transcriptomic and metabolomic data identified AA metabolism, ferroptosis, fatty acid biosynthesis, glycerophospholipid metabolism, and ABC transporters as significantly enriched pathways (Figure 3C).

3.5. Probiotics Alleviate NP-Induced Liver Injury via Coordinated Suppression of Ferroptosis and Remodeling of AA Metabolism

Integrated transcriptomic and metabolomic analyses, together with a mechanistic study, suggested that probiotic supplementation may have restored NP-induced hepatic dysfunction by reshaping the "host gene–metabolite" axis, thereby potentially maintaining hepatic metabolic homeostasis (Figure 4). Probiotics appeared to coordinately regulated iron metabolism and oxidative stress: they showed upregulation of iron-binding protein gene *hpxa*, likely reducing free Fe^{3+} toxicity; and downregulated *steap4*, suppressing the reduction of Fe^{3+} to Fe^{2+}, which could decrease mitochondrial reactive oxygen species (ROS) production via the Fenton reaction ($Fe^{2+} + H_2O_2 \rightarrow OH\cdot + OH^- + Fe^{3+}$), thus potentially curbing oxidative damage at its source. Meanwhile, probiotics differentially modulated the three major pathways of AA metabolism: (1) LOX pathway: Given that

LOX catalytic activity depends on Fe^{2+}/Fe^{3+}, probiotics downregulated *alox12* expression; together with the reduced Fe^{2+} availability resulting from *steap4* downregulation, this could synergistically decrease the production of downstream 12HPETE and MDA (AA—*alox12*↓—(Fe^{3+}↓) → 12-HPETE—(Fe^{2+}↓) → MDA↓), effectively suppressing lipid peroxidation. (2) CYP450 pathway: Probiotics upregulated *cyp2j* expression, promoting the production of the anti-inflammatory metabolite 11,12EET (AA—(*cyp2j*↑) → 11,12-EET↑). (3) COX pathway: Probiotics downregulated *ptgs2a* (encoding COX2), potentially inhibiting the production of the pro-inflammatory factor PGE_2 (AA—(*ptgs2a*↓) → PGG_2 → PGH_2 → PGE_2↓). In summary, probiotics alleviate NP-induced oxidative stress and inflammatory injury by reestablishing a complete metabolic regulatory network that integrates iron homeostasis modulation and synergistic reprogramming of the three AA pathways (LOX, CYP450, COX), thereby systematically restoring hepatic metabolic and inflammatory homeostasis.

3.6. Probiotics Alleviate NP-Induced Liver Injury by Restoring Hepatic Triglyceride Synthesis

Probiotic intervention appeared to systematically restore the NP-suppressed hepatic triglyceride (TG) synthesis pathway and potentially reestablish lipid metabolic homeostasis (Figure 5). Probiotic treatment significantly upregulated *acsl4a*, suggesting promotion of the conversion of fatty acids to acyl-CoA and providing activated acyl donors for subsequent esterification reactions. While ACSL4 is traditionally viewed as a pro-ferroptotic enzyme, its biological output is context-dependent: ACSL4 upregulation does not automatically drive ferroptosis; rather, the outcome depends on the downstream metabolic fate of activated fatty acids. The restorative process drove TG synthesis through the following four sequential steps: (1) reduction: probiotics upregulated *gpd1b*, facilitating the conversion of dihydroxyacetone phosphate (DHAP) to glycerol3phosphate (G3P), a critical step in TG synthesis; (2) acylation: upregulated *gpat3* converted G3P to lysophosphatidic acid (LPA) through acylation; (3) second acylation: upregulated *agpat6* mediated the acyl transfer from LPA to phosphatidic acid (PA), completing PA synthesis; (4) esterification: with *acsl4a* upregulation ensuring sufficient acyl-CoA supply, the markedly upregulated *dgat2* drove the conversion of diacylglycerol (DAG) to the end product TG (summarized as DHAP - (*gpd1b*↑) → G3P↑—(*gpat3*↑) → LPA—(*agpat6*↑) → PA—(*plpp7*↑) → DAG↑—(*dgat2*↑) → TG↑). In summary, probiotics alleviate NP-induced lipid metabolic disorders by re-establishing a complete metabolic cascade that spans from substrate supply to the coordinated upregulation of key genes, thereby systematically promoting TG synthesis.

3.7. RT-qPCR Validation of DEGs

Five DEGs (*sod1*, *cat*, *gpx4a*, *igfbp1b*, and *hpxa*) were selected for RT-qPCR analysis, with the RT-qPCR results showing that expression patterns consistent with RNA-Seq results (Figure 6). Compared to the Control group, NP exposure significantly reduced *sod1*, *cat*, *gpx4a*, and *hpxa* expression, whereas *igfbp1b* was significantly increased ($p < 0.05$). In the NP-Pro group, *sod1*, *cat*, *gpx4a*, and *hpxa* expression levels significantly increased, while *igfbp1b* significantly decreased ($p < 0.05$), with all four genes returning to levels close to those observed in the Control group.

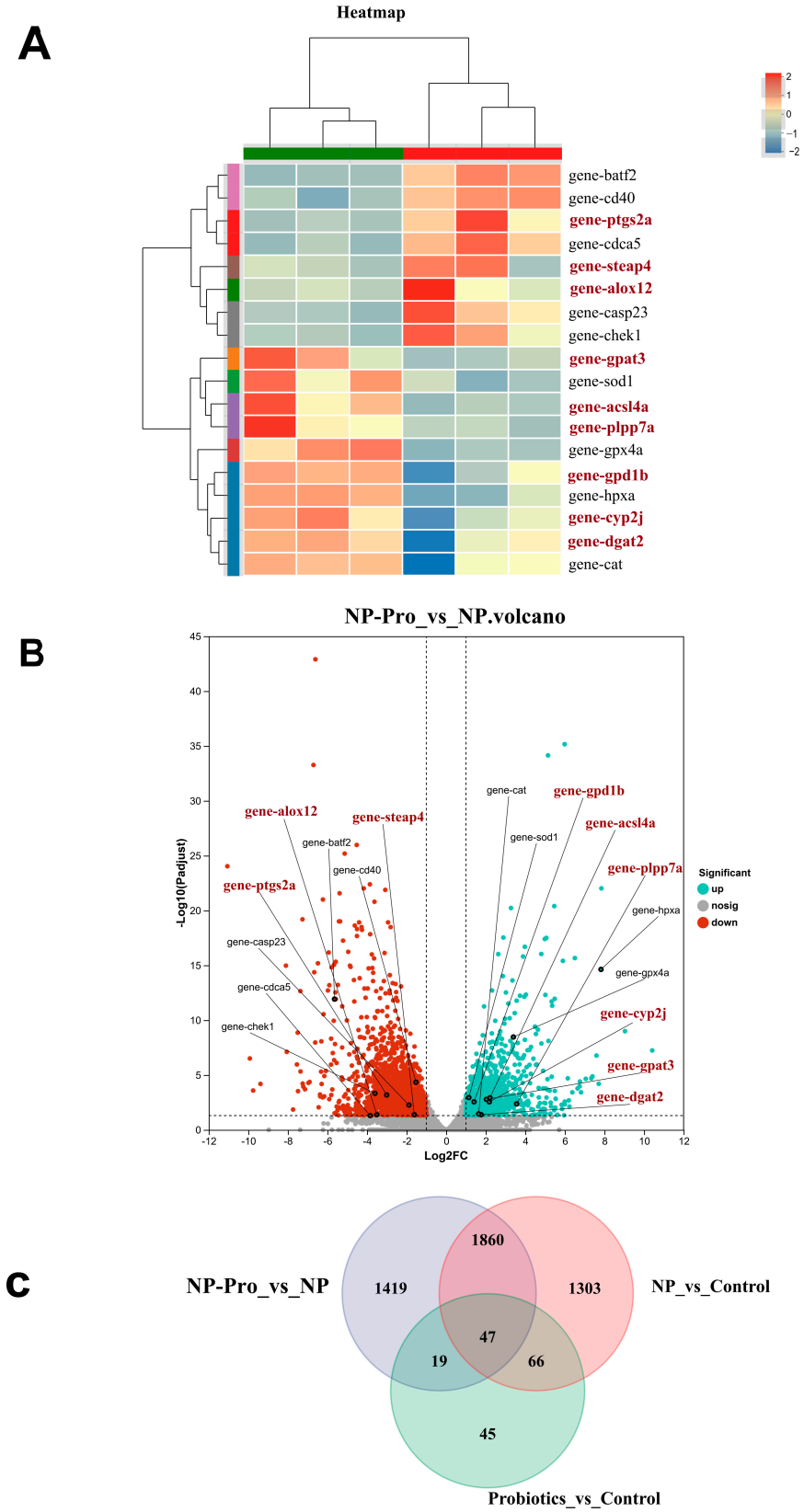

Figure 1. NP-Pro intervention significantly reversed the abnormal liver gene expression induced by NP exposure in *S. meridionalis*: (**A**) heatmap of genes in NP-Pro vs. NP; (**B**) volcano plot of DEGs between NP-Pro and NP. The dashed vertical lines indicate the fold-change threshold of $|\log2FC| \geq 1$, and genes with adjusted $p < 0.05$ are considered significantly differentially expressed. (**C**) Venn diagram of shared DEGs across three comparisons. Note: red font indicates genes involved in the AA pathway, ferroptosis, or TG synthesis.

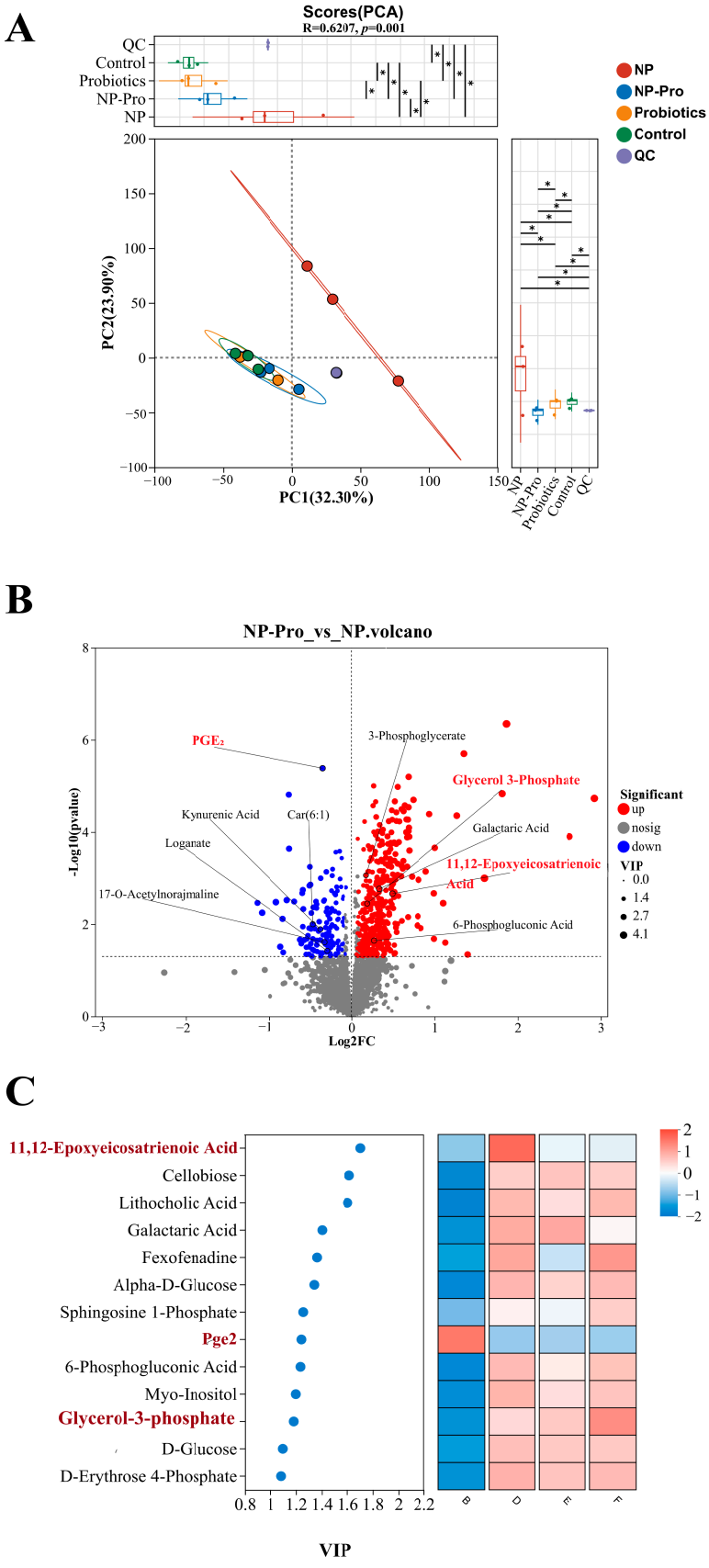

Figure 2. Metabolomic profiling of liver metabolic changes after probiotics intervention: (**A**) PCA score plot of metabolic profiles, * in the figure denotes statistically significant differences between compared groups ($p < 0.05$); (**B**) volcano plot of differential metabolites (NP-Pro vs. NP); (**C**) heatmap of metabolite abundance across NP-Pro vs. NP group.

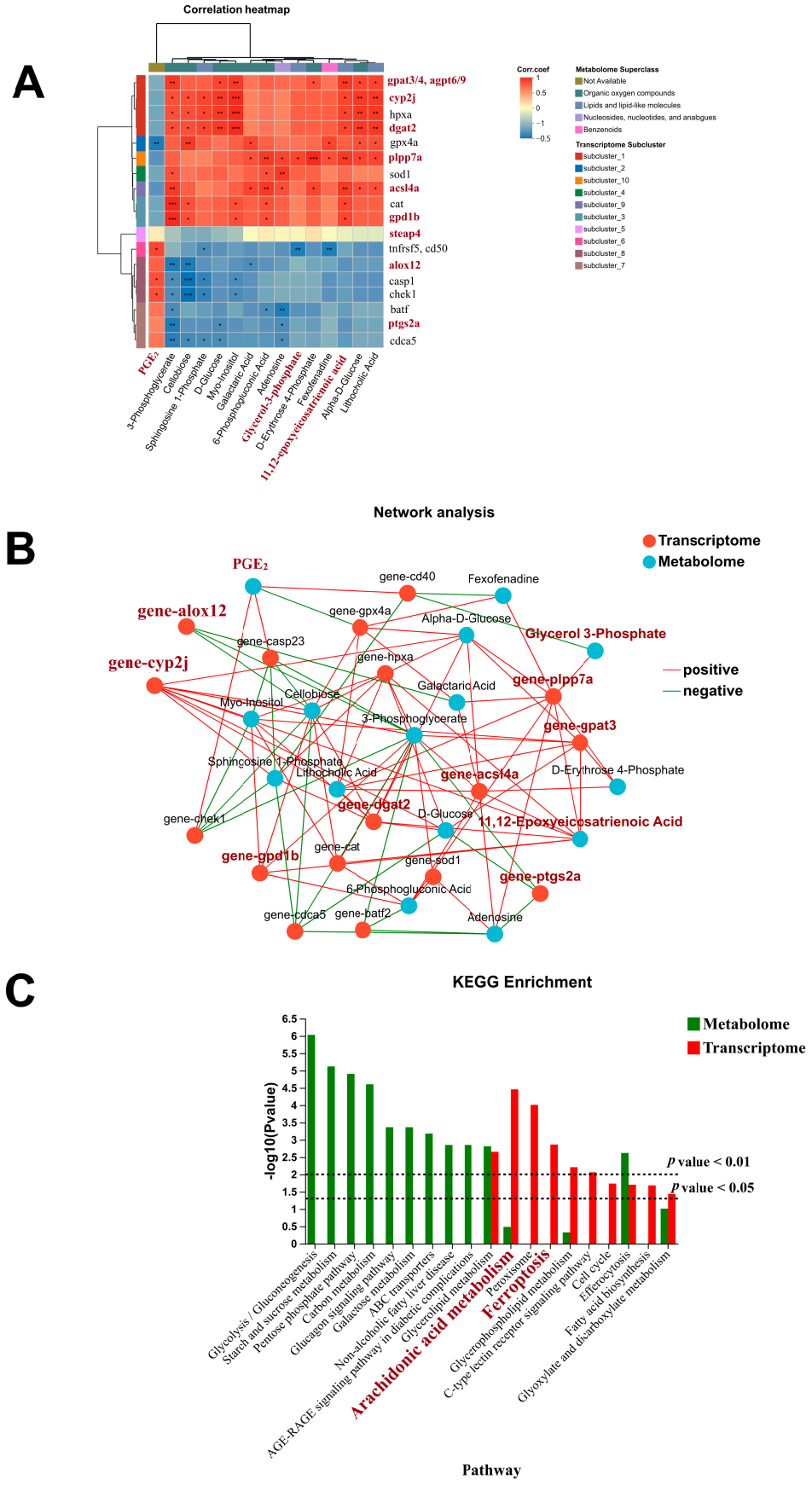

Figure 3. Integrated transcriptomic and metabolomic analysis of the liver of *S. meridionalis* under NP-Pro intervention: (**A**) correlation heatmap of associations between DEGs and characteristic metabolites. Asterisks represent significance levels of correlation coefficients: *, $p < 0.05$; **, $p < 0.01$;

***, $p < 0.001$, red font indicates genes involved in the AA pathway, ferroptosis, or TG synthesis, and metabolites involved in AA metabolism or TG synthesis; (**B**) gene–metabolite network of the synergistic regulation among key pathway molecules; (**C**) KEGG enrichment showing arachidonic acid metabolism and ferroptosis as coenriched core pathways. Red font indicates that both transcriptomic and metabolomic datasets are significantly enriched in arachidonic acid metabolism and ferroptosis pathways.

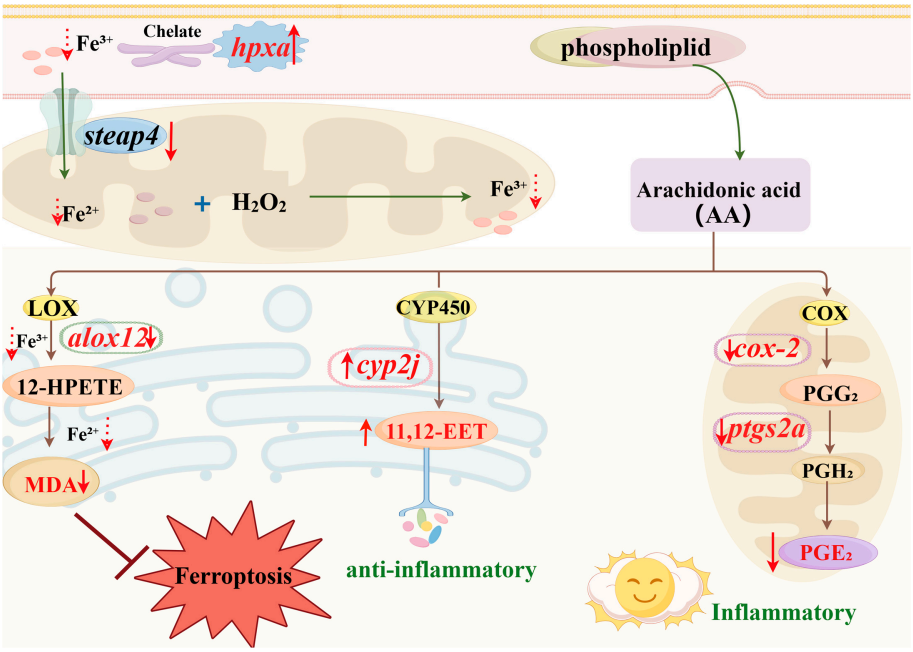

Figure 4. Schematic illustration of the molecular regulatory network involving the ferroptosis pathway and three branches of AA metabolism. Note: This schematic was created using Figdraw 2.0. Notes: red solid arrows indicate genes and metabolites involved in the AA pathway or ferroptosis; red dashed arrows indicate putative Fe ions that have not been experimentally verified.

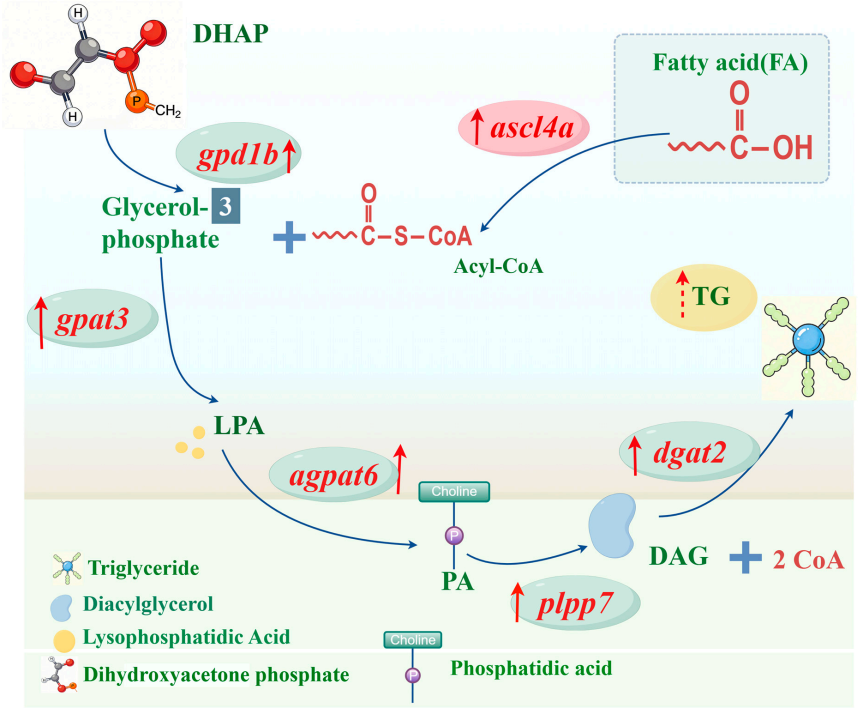

Figure 5. Schematic illustration of triglyceride biosynthesis. Note: red solid arrows indicate genes involved in TG synthesis; red dashed arrows indicate unverified metabolite TG.

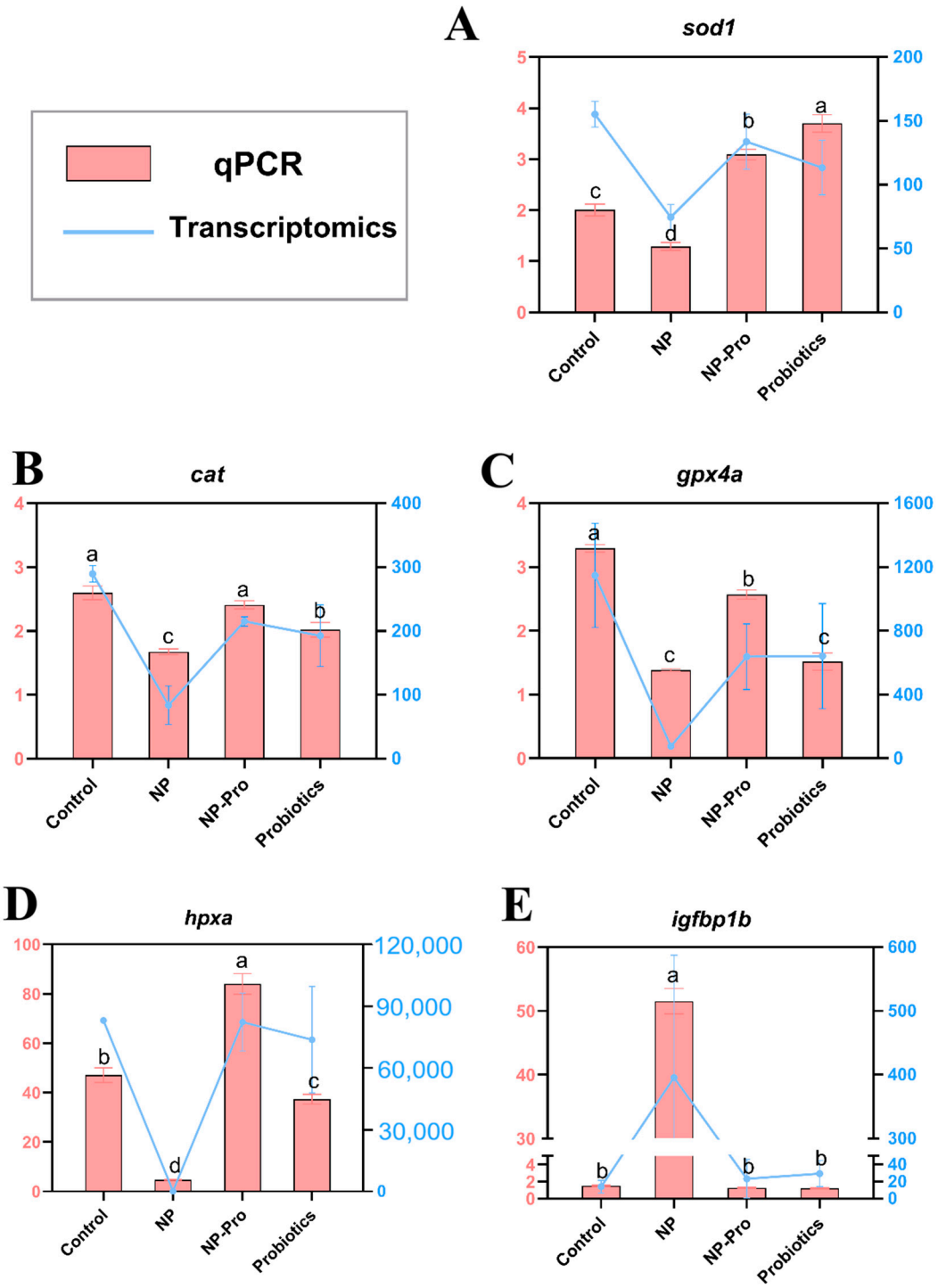

Figure 6. Validation of five DEGs by RT-qPCR. (**A**) *sod1*; (**B**) *cat*; (**C**) *gpx4a*; (**D**) *hpxa*; (**E**) *igfbp1b*. The *X*-axis represents four different experimental groups. The left *Y*-axis indicates the relative mRNA expression levels of each gene across the four groups measured by RT-qPCR, while the right *Y*-axis indicates the Fragments Per Kilobase of exon model per Million mapped fragments (FPKM) values for each gene across the four groups as determined by transcriptomics. Different superscript letters (a, b, c, d) denote significant intergroup differences in RT-qPCR data, $p < 0.05$.

4. Discussion

Integrated transcriptomic and metabolomic analyses identified that NP-induced hepatotoxicity in *S. meridionalis* is centered on ferroptosis, suggesting that oxidative stress and AA metabolism disruption, along with suppressed TG synthesis, may play central

roles in this process. Probiotic pretreatment effectively reversed these effects through systemic metabolic reprogramming, highlighting its potential as a mitigation strategy against emerging pollutant exposure in aquatic organisms.

NP-induced hepatotoxicity was closely linked to ferroptosis. In this study, NP exposure lowered antioxidant enzyme activities (SOD, CAT) and raised ROS and MDA levels in *S. meridionalis*, consistent with previous reports in zebrafish [24]. Consistent NP-mediated suppression of antioxidant defenses and hepatic histopathological lesions have also been reported in *Salmo caspius* [25]. In *O. niloticus*, thermal stress synergistically exacerbates oxidative injury triggered by 4-NP [26]. These findings corroborate our results and suggest that NP-induced oxidative stress is a conserved response across fish species, while also indicating that additional environmental stressors may potentiate its toxicity in natural ecosystems. This oxidative state was accompanied by iron dyshomeostasis, as evidenced by upregulated *steap4* expression and subsequent Fe^{2+} overload. Excess ROS then attacked AA-rich membrane phospholipids, triggering lipid peroxidation, a hallmark of ferroptosis [27,28]. Concurrently, NP suppressed *gpx4a* expression, a key inhibitor of ferroptosis, weakening the cellular defense against lipid peroxidation. This NP-induced ferroptosis matches findings in mammalian cells [29], suggesting that this cell death pathway may represent a conserved response to NP exposure across vertebrates. From an ecological risk assessment perspective, these findings highlight several potential biomarkers (e.g., iron homeostasis disruption, *gpx4a* suppression) that may be useful for monitoring NP toxicity in aquatic ecosystems.

The disruption of AA metabolism appeared as another potential axis of NP hepatotoxicity. AA metabolism is not a linear cascade but a branched network generating functionally diverse and sometimes opposing lipid mediators. LOX metabolites encompass both pro-inflammatory leukotrienes and pro-resolving lipoxins, whereas EETs display tissue-dependent activities [30]. Given this complexity, the NP-induced alterations we observed should be interpreted as a net shift in the metabolic equilibrium across the AA network, rather than unidirectional activation or inhibition of individual pathways. Our data suggested that NP was associated with activation of the pro-inflammatory COX pathway (*ptgs2a* → PGE_2) and LOX pathway (*alox12* → MDA), while suppression of the anti-inflammatory CYP450 pathway (*cyp2j* → 11,12-EET) was also observed. This imbalance may contribute to the accumulation of lipid peroxides, potentially establishing a ferroptosis–inflammation feedforward loop that could exacerbate liver injury. This observation is consistent with earlier findings that NP disrupts AA metabolism [31] and extends them by revealing the concurrent modulation of all three major AA pathways in fish liver. Notably, NP was also associated with suppression of the TG synthesis axis (DHAP → G3P → LPA → PA → DAG → TG), reducing the cellular energy buffer capacity [32]. This metabolic suppression may represent an adaptive response to energy stress, yet it could concurrently impair the liver's regenerative capacity [33]. Interestingly, this pattern contrasts with a study reporting that NP induces lipid accumulation in *Caenorhabditis elegans* by promoting lipogenesis and inhibiting lipolysis [34]. This opposing finding suggests species-specific differences in the metabolic effects of NP, highlighting the need for further investigation to improve the reliability of cross-species risk extrapolation.

Probiotic pretreatment was associated with the reversal of these NP-induced pathological alterations. Probiotics restored antioxidant enzyme activity; reduced hepatic Fe^{2+}, MDA, and H_2O_2 levels; and upregulated *gpx4a* expression, directly counteracting lipid peroxides. This finding aligns with the known role of GPX4 in blocking ferroptosis [35]. Simultaneously, probiotics downregulated pro-inflammatory genes (*alox12*, *ptgs2a*) and metabolite PGE_2, while upregulating *cyp2j* and the anti-inflammatory metabolite 11,12-EET, consistent with previous studies on probiotics and AA metabolism [36]. Beyond these

effects on oxidative stress and inflammation, probiotics showed multi-target effects on lipid metabolism. Probiotics increased *acsl4a* expression, a finding that appears paradoxical given that ACSL4 is traditionally viewed as a pro-ferroptotic enzyme that incorporates polyunsaturated fatty acids (PUFAs) into membrane lipids [37]. However, ACSL4 functions as a context-dependent metabolic switch rather than a static pro-ferroptotic factor; its biological output depends on substrate flux partitioning. This coordinated response represents a lipid sequestration mechanism, wherein ACSL4-activated PUFAs are channeled into TG storage rather than membrane phospholipids, thereby depleting the PUFA pool available for peroxidation and ferroptosis execution [38,39]. Thus, despite *acsl4a* upregulation, ferroptosis could be suppressed due to redirection of substrate flux toward storage rather than membrane incorporation. In this study, probiotics simultaneously upregulated key enzymes of the TG synthesis pathway (*gpd1b*, *gpat3*, *agpat6*, *dgat2*). This coordinated "lipid sequestration" process offers two benefits: it removes toxic free fatty acids, reducing lipotoxicity, and depletes the PUFA pool, thereby cutting off the source of pro-inflammatory signals and ferroptosis. This fits with the emerging view that lipid droplets help control ferroptotic signals [40]. Interestingly, while certain probiotics suppress ferroptosis by directly downregulating ACSL4 [41], the present study reveals a distinct feature—*acsl4a* activation coupled with TG synthesis enhancement—suggesting functional divergence in probiotic-mediated ferroptosis inhibition that may have implications for species-specific probiotic applications.

This study has several limitations. First, the exposure time was limited, and broader dose- and time-dependent effects remain to be explored; second, due to the limited RNA yield from the same liver used for transcriptome library construction, qPCR validation of key AA-related genes (e.g., *ptgs2a*, *alox12*, *cyp2j*, *steap4*, *dgat2*) was not feasible; third, the current exploratory screening had a limited sample size (n = 3 per platform). However, 11 preserved specimens per group have been retained for future targeted validation (qPCR of hub genes and MRM-based metabolomics), which will provide more robust statistical confirmation with n = 5–6 per group.

5. Conclusions

Integrated transcriptomic and metabolomic analyses provide correlative evidence that probiotics may alleviate NP-induced hepatotoxicity in *S. meridionalis* through a potential triple-axis mechanism involving restoration of iron homeostasis, AA metabolic rebalancing (with suppression of pro-inflammatory COX/LOX pathways and enhancement in the anti-inflammatory CYP450 branch), and TG replenishment via the DHAP-to-TG cascade. These coordinated changes may attenuate the inflammation–ferroptosis feedforward loop and redirect free fatty acids toward stable TG storage, potentially mitigating lipotoxicity and reducing pro-ferroptotic PUFA availability. However, as our evidence is largely indirect and important ferroptosis markers were not assessed, the proposed mechanisms should be regarded as correlative and hypothetical, warranting experimental confirmation (e.g., via pharmacological inhibition or genetic approaches). Nevertheless, these findings provide a correlative foundation for NP risk assessment and suggest that modulating host-ecology may help mitigate the health effects of emerging pollutants in aquatic ecosystems.

Supplementary Materials: The following supporting information can be downloaded at: https://www.mdpi.com/article/10.3390/fishes11080473/s1, Supplementary Figure S1: Experimental design.

Author Contributions: D.L.: Writing—review & editing, Writing—original draft, Investigation. F.L.: Writing—original draft, Validation. L.Y.: Writing—review & editing, Validation. Z.G.: Data curation, Conceptualization. X.Z.: Formal analysis. R.D.: Writing—review & editing, Writing—

original draft, Validation, Project administration, Investigation, Funding acquisition, Data curation, Conceptualization. All authors have read and agreed to the published version of the manuscript.

Funding: This work was financially supported by grants from the National Natural Science Foundation of China (32460918), Guizhou Modern Agricultural Industry Technology System of China (GZSTYYCYJSTX-202605).

Institutional Review Board Statement: The animal study protocol was approved by the Experimental Animal Ethics Committee of Guizhou University (protocol code EAE-GZU-2024-T103 and approval date: 14 March 2024).

Data Availability Statement: Data is provided within the manuscript. The raw sequence data reported in this study have been deposited in the GSA and OMIX databases at the National Genomics Data Center (NGDC), China National Center for Bioinformation/Beijing Institute of Genomics, Chinese Academy of Sciences. The accession numbers for the transcriptomic, and metabolomic data are CRA037040 and OMIX014312 respectively, via the following URLs: https://ngdc.cncb.ac.cn/gsa and https://ngdc.cncb.ac.cn/omix (accessed on 10 August 2026).

Conflicts of Interest: The authors declare no conflict of interest.

Abbreviations

NP: Nonylphenol; AA: arachidonic acid; TG: triglyceride; G3P: glycerol-3-phosphate; LPA: lysophosphatidic acid; PA: phosphatidic acid; DAG: diacylglycerol; RT-qPCR: reverse transcription quantitative real-time PCR; ELISA: enzyme-linked immunosorbent assay; MDA: malondialdehyde; SOD: superoxide dismutase; CAT: catalase; H_2O_2: hydrogen peroxide; 11,12-EET: 11,12-epoxyeicosatrienoic acid; DEGs: differentially expressed genes; DHAP: dihydroxyacetone phosphate; FDR: false discovery rate; *acsl4a*: acyl-CoA synthetase long chain family member 4a; *dgat1b*: diacylglycerol O-acyltransferase 1b; *gpd1b*: glycerol-3-phosphate dehydrogenase 1b; *agpat6*: 1-acylglycerol-3-phosphate O-acyltransferase 6; *gpat3*: glycerol-3-phosphate acyltransferase 3; *cyp2j*: cytochrome P450 family 2 subfamily J; *alox12*: arachidonate 12-lipoxygenase; *steap4*: STEAP family member 4; *plpp7a*: phospholipid phosphatase 7a.

References

1. Zahid, B.M.; Nurulnadia, M.Y. Occurrence, Partitioning Behavior, and Ecological Risk Assessment of Octylphenol and Nonylphenol in Surface Waters and Sediments of Terengganu Rivers, Malaysia. *Environ. Monit. Assess.* **2025**, *197*, 546. [CrossRef] [PubMed]
2. Zheng, M.; Li, S.; Xu, J.; Luo, Y.; He, J.; Wang, C.; Xu, Y.; Zeng, Y.; Yu, J. Nonylphenol Exposure Induces Myocardial Fibrosis via the RhoA/ROCK1/MLC-Signaling Pathway. *Ecotoxicol. Environ. Saf.* **2025**, *299*, 118423. [CrossRef] [PubMed]
3. Vieira, C.E.D.; Tesser, M.E.; Meletti, P.C.; dos Reis Martinez, C.B. Chronic In-Situ Exposure to Pesticide-Contaminated Water Bodies Impairs the Metabolism, Growth, and Performance of the Freshwater Fish *Prochilodus lineatus*. *Sci. Total Environ.* **2025**, *995*, 180085. [CrossRef] [PubMed]
4. Sun, D.; Chen, Q.; Zhu, B.; Zhao, H.; Duan, S. Multigenerational Reproduction and Developmental Toxicity, and HPG Axis Gene Expression Study on Environmentally-Relevant Concentrations of Nonylphenol in Zebrafish. *Sci. Total Environ.* **2021**, *764*, 144259. [CrossRef] [PubMed]
5. Zhang, J.; Liu, L.; Ning, X.; Lin, M.; Lai, X. Isomer-Specific Analysis of Nonylphenol and Their Transformation Products in Environment: A Review. *Sci. Total Environ.* **2023**, *901*, 165982. [CrossRef] [PubMed]
6. Simón, R.; Docando, F.; Nuñez-Ortiz, N.; Tafalla, C.; Díaz-Rosales, P. Mechanisms Used by Probiotics to Confer Pathogen Resistance to Teleost Fish. *Front. Immunol.* **2021**, *12*, 653025. [CrossRef] [PubMed]
7. Giommi, C.; Santoni, C.; Carli, F.; Gastaldelli, A.; Maradonna, F.; Habibi, H.R.; Giorgini, E.; Carnevali, O. BPA Disrupts Hepatic Lipid and Carbohydrate Metabolism in Female Zebrafish: Protective Effects of Probiotics Revealed by FTIRI and Lipidomics. *Int. J. Mol. Sci.* **2026**, *27*, 2978. [CrossRef] [PubMed]
8. Huo, Y.; Wang, Y.; Ma, N.; Guo, Y.; Khan, A.; Mai, W. Dietary Supplementation of *Lactobacillus casei* Alleviates Permethrin Exposure-Induced Zebrafish Testis Damage through Modulation of TLR4/NF-κB and AKT/Nrf2 Pathways: Oxidative Stress, Inflammation and Ferroptosis. *Pestic. Biochem. Physiol.* **2025**, *212*, 106450. [CrossRef] [PubMed]

9. Li, J.; Cen, J.; Zhou, Q.; Zheng, X.; Wu, Z.; Li, Z.; Wang, Y.; Jiang, L.; Sun, C.; Liu, B. Dietary Probiotic Intervention Strategies of *Lactobacillus acidophilus* and *Bacillus subtilis* Co-Cultured in *Litopenaeus vannamei* with Low Fishmeal Diet: Insights from Immune Enhancement, Anti-*Vibrio* and Ammonia Nitrogen Stress. *Fish Shellfish Immunol.* **2025**, *164*, 110414. [CrossRef] [PubMed]
10. Nasr, R.; Ayaat, A.N.; Abd El Ghaffar, H.A. Effect of a Mixture of Probiotics (*Pediococcus acidilactici*, *Lactobacillus acidophilus*, and *Bacillus subtilis*) on the Physiological Status and Fish Health of the Nile Tilapia (*Oreochromis niloticus*). *Egypt. J. Aquat. Biol. Fish.* **2025**, *29*, 2689. [CrossRef]
11. Zhang, Q.; Hou, S.; Liu, Y.; Du, J.; Jia, Y.; Yang, Q.; Xu, T.; Takagi, Y.; Li, D.; Zhang, X. Properties of Skin Collagen from Southern Catfish (*Silurus meridionalis*) Fed with Raw and Cooked Food. *Foods* **2024**, *13*, 2901. [CrossRef] [PubMed]
12. Li, J.; Xie, X. Inconsistent Responses of Liver Mitochondria Metabolism and Standard Metabolism in *Silurus meridionalis* When Exposed to Waterborne Cadmium. *Comp. Biochem. Physiol. Part C Toxicol. Pharmacol.* **2018**, *214*, 17–22. [CrossRef] [PubMed]
13. Mbokane, E.M.; Moyo, N.A.G. Use of Medicinal Plants as Feed Additives in the Diets of Mozambique Tilapia (*Oreochromis mossambicus*) and the African Sharptooth Catfish (*Clarias gariepinus*) in Southern Africa. *Front. Vet. Sci.* **2022**, *9*, 1072369. [CrossRef] [PubMed]
14. Wang, L.; Sagada, G.; Wang, C.; Liu, R.; Li, Q.; Zhang, C.; Yan, Y. Exogenous Bile Acids Regulate Energy Metabolism and Improve the Health Condition of Farmed Fish. *Aquaculture* **2023**, *562*, 738852. [CrossRef]
15. Mathew, R.T.; Alkhamis, Y.A.; Saud Alsaqufi, A.; Mansour, A.T.; Ganesan, N.; Mabrok, M.; Abdul Kari, Z.; Eissa, M.E.H.; Almutairi, L.A.; Eissa, E.-S.H. Supplementation of Multi-Strain Probiotics in Water Enhances Growth, Metabolic Responses, Immune Function, Growth and Immunity Genes, and Disease Resistance in Nile Tilapia (*Oreochromis niloticus*). *Aquacult. Int.* **2025**, *33*, 407. [CrossRef]
16. Ye, Z.; Yu, L.; Lu, D.; Zhang, Q.; Narbad, A.; Chen, W.; Zhai, Q.; Tian, F. Mitigating Effect of *Bifidobacterium longum* CCFM1077 on Nonylphenol Toxicity: An Integrative *in Vitro* and *in Vivo* Analysis. *J. Hazard. Mater.* **2024**, *480*, 136401. [CrossRef] [PubMed]
17. Abd-Elkareem, M.; Sayed, A.E.-D.H.; Khalil, N.S.A.; Kotob, M.H. Nigella Sativa Seeds Mitigate the Hepatic Histo-Architectural and Ultrastructural Changes Induced by 4-Nonylphenol in *Clarias gariepinus*. *Sci. Rep.* **2023**, *13*, 4109. [CrossRef] [PubMed]
18. Eid, Z.; Mahmoud, U.M.; Mekkawy, I.A.A.; Abdel-Tawab, H.S.; Sayed, A.E.-D.H. 4-Nonylphenol Induced Brain Damage in Juvenile African Catfish (*Clarias garepinus*). *Toxicol. Environ. Health Sci.* **2021**, *13*, 201–214. [CrossRef]
19. Standen, B.T.; Rawling, M.D.; Davies, S.J.; Castex, M.; Foey, A.; Gioacchini, G.; Carnevali, O.; Merrifield, D.L. Probiotic *Pediococcus acidilactici* Modulates Both Localised Intestinal- and Peripheral-Immunity in Tilapia (*Oreochromis niloticus*). *Fish Shellfish Immunol.* **2013**, *35*, 1097–1104. [CrossRef] [PubMed]
20. Li, X.; Wang, S.; Zhang, M.; Li, M.; Chen, C. Integrated Transcriptomic and Metabolomic Analysis Elucidates the Impact of Acute Ammonia Stress on Carbohydrate and Lipid Metabolic Pathways in Yellow Catfish (*Pelteobagrus fulvidraco*). *Aquac. Nutr.* **2025**, *2025*, 5545977. [CrossRef] [PubMed]
21. Jin, M.; Zheng, A.; Mkulo, E.M.; Wang, L.; Zhang, H.; Tang, B.; Zhou, H.; Wang, B.; Huang, J.; Wang, Z. Metabolomics-Based Analysis of Adaptive Mechanism of *Eleutheronema tetradactylum* to Low-Temperature Stress. *Animals* **2025**, *15*, 1174. [CrossRef] [PubMed]
22. Rachid Zaim, S.; Kenost, C.; Berghout, J.; Vitali, F.; Zhang, H.H.; Lussier, Y.A. Evaluating Single-Subject Study Methods for Personal Transcriptomic Interpretations to Advance Precision Medicine. *BMC Med. Genom.* **2019**, *12*, 96. [CrossRef] [PubMed]
23. Sun, Q.; Huang, X.; Long, H.; Guo, J.; Zhang, R.; Lu, D.; Yao, H.; Jiang, K.; Pi, Y. Dysregulation of Glu-GABA and Reduction of Triglycerides Contribute to Valproic Acid-Induced Autism Model in Zebrafish. *J. Lipid Res.* **2025**, *66*, 100911. [CrossRef] [PubMed]
24. Desai, J.K.; Trangadia, B.J.; Patel, U.D.; Patel, H.B.; Kalaria, V.A.; Kathiriya, J.B. Neurotoxicity of 4-Nonylphenol in Adult Zebrafish: Evaluation of Behaviour, Oxidative Stress Parameters and Histopathology of Brain. *Environ. Pollut.* **2023**, *334*, 122206. [CrossRef] [PubMed]
25. Shirdel, I.; Kalbassi, M.R.; Esmaeilbeigi, M.; Tinoush, B. Disruptive Effects of Nonylphenol on Reproductive Hormones, Antioxidant Enzymes, and Histology of Liver, Kidney and Gonads in Caspian Trout Smolts. *Comp. Biochem. Physiol. Part C Toxicol. Pharmacol.* **2020**, *232*, 108756. [CrossRef] [PubMed]
26. Shaalan, W.M.; Elbaghdady, H.A.M.; Sayed, A.E.-D.H. Synergistic Effects of Thermal Stress and 4-Nonylphenol on Oxidative Stress and Immune Responses in Juvenile Tilapia (*Oreochromis niloticus*). *Environ. Sci. Pollut. Res.* **2024**, *31*, 64024–64032. [CrossRef] [PubMed]
27. Liang, D.; Minikes, A.M.; Jiang, X. Ferroptosis at the Intersection of Lipid Metabolism and Cellular Signaling. *Mol. Cell* **2022**, *82*, 2215–2227. [CrossRef] [PubMed]
28. Zheng, D.; Liu, J.; Piao, H.; Zhu, Z.; Wei, R.; Liu, K. ROS-Triggered Endothelial Cell Death Mechanisms: Focus on Pyroptosis, Parthanatos, and Ferroptosis. *Front. Immunol.* **2022**, *13*, 1039241. [CrossRef] [PubMed]
29. Zhang, X.; Yan, W.; Chen, X.; Li, X.; Yu, B.; Zhang, Y.; Ding, B.; Hu, J.; Liu, H.; Nie, Y.; et al. Long-Term 4-Nonylphenol Exposure Drives Cervical Cell Malignancy through MAPK-Mediated Ferroptosis Inhibition. *J. Hazard. Mater.* **2024**, *471*, 134371. [CrossRef] [PubMed]

30. Capdevila, J.H.; Falck, J.R.; Adebesin, A.M. Epoxyeicosatrienoic Acids (EETs): A Novel Class of Second Messengers of Hormonal Functional Responses. *Prostaglandins Other Lipid Mediat.* **2025**, *177*, 106967. [CrossRef] [PubMed]
31. Fujimoto, Y.; Sakuma, S.; Inoue, T.; Uno, E.; Fujita, T. The Endocrine Disruptor Nonylphenol Preferentially Blocks Cyclooxygenase-1. *Life Sci.* **2002**, *70*, 2209–2214. [CrossRef] [PubMed]
32. Sharma, A.; Anand, S.K.; Singh, N.; Dwivedi, U.N.; Kakkar, P. AMP-Activated Protein Kinase: An Energy Sensor and Survival Mechanism in the Reinstatement of Metabolic Homeostasis. *Exp. Cell Res.* **2023**, *428*, 113614. [CrossRef] [PubMed]
33. Yu, J.; Yang, X.; Yang, X.; Yang, M.; Wang, P.; Yang, Y.; Yang, J.; Li, W.; Xu, J. Nonylphenol Aggravates Non-Alcoholic Fatty Liver Disease in High Sucrose-High Fat Diet-Treated Rats. *Sci. Rep.* **2018**, *8*, 3232. [CrossRef] [PubMed]
34. Liu, F.; Cao, X.; Zhou, L. Lipid Metabolism Analysis Providing Insights into Nonylphenol Multi-Toxicity Mechanism. *iScience* **2023**, *26*, 108417. [CrossRef] [PubMed]
35. Liang, H.; Chen, S.; Zhong, J.; Chen, X.; Xie, T.; Chen, Z.; Bai, Z.; Yuan, J.; Jiang, P.; Zhao, X.; et al. Dapagliflozin Improves Diabetic Nephropathy by Regulating Autophagy and Ferroptosis through CYP450s/ROS Pathway. *Biochem. Pharmacol.* **2025**, *240*, 117134. [CrossRef] [PubMed]
36. Zhu, J.; Liu, W.; Bian, Z.; Ma, Y.; Kang, Z.; Jin, J.; Li, X.; Ge, S.; Hao, Y.; Zhang, H.; et al. Lactobacillus Plantarum Zhang-LL Inhibits Colitis-Related Tumorigenesis by Regulating Arachidonic Acid Metabolism and CD22-Mediated B-Cell Receptor Regulation. *Nutrients* **2023**, *15*, 4512. [CrossRef] [PubMed]
37. Doll, S.; Proneth, B.; Tyurina, Y.Y.; Panzilius, E.; Kobayashi, S.; Ingold, I.; Irmler, M.; Beckers, J.; Aichler, M.; Walch, A.; et al. Acsl4 Dictates Ferroptosis Sensitivity by Shaping Cellular Lipid Composition. *Nat. Chem. Biol.* **2017**, *13*, 91–98. [CrossRef] [PubMed]
38. Lee, H.; Horbath, A.; Kondiparthi, L.; Meena, J.K.; Lei, G.; Dasgupta, S.; Liu, X.; Zhuang, L.; Koppula, P.; Li, M.; et al. Cell Cycle Arrest Induces Lipid Droplet Formation and Confers Ferroptosis Resistance. *Nat. Commun.* **2024**, *15*, 79. [CrossRef] [PubMed]
39. Dixon, S.J.; Olzmann, J.A. The Cell Biology of Ferroptosis. *Nat. Rev. Mol. Cell Biol.* **2024**, *25*, 424–442. [CrossRef] [PubMed]
40. Jovičić, E.J.; Janež, A.P.; Eichmann, T.O.; Koren, Š.; Brglez, V.; Jordan, P.M.; Gerstmeier, J.; Lainšček, D.; Golob-Urbanc, A.; Jerala, R.; et al. Lipid Droplets Control Mitogenic Lipid Mediator Production in Human Cancer Cells. *Mol. Metab.* **2023**, *76*, 101791. [CrossRef] [PubMed]
41. Zhao, Q.; Lai, J.; Jiang, Y.; Cui, E.; Chang, H.; Pan, R.; Li, P.; Shao, J.-Z.; Zheng, J.; Chen, Y. Lactiplantibacillus Plantarum-Derived Extracellular Vesicles Alleviate Acute Lung Injury by Inhibiting Ferroptosis of Macrophages. *J. Nanobiotechnol.* **2025**, *23*, 307. [CrossRef] [PubMed]

Disclaimer/Publisher's Note: The statements, opinions and data contained in all publications are solely those of the individual author(s) and contributor(s) and not of MDPI and/or the editor(s). MDPI and/or the editor(s) disclaim responsibility for any injury to people or property resulting from any ideas, methods, instructions or products referred to in the content.